Heliyon

ELSEVIER

Received:
4 May 2016
Revised:
24 August 2016
Accepted:
14 November 2016

Heliyon 2 (2016) e00199

An assessment of the evaporation and condensation phenomena of lithium during the operation of a Li(d,xn) fusion relevant neutron source

J. Knaster [a,*], **T. Kanemura** [b,1], **K. Kondo** [b]

[a] *IFMIF/EVEDA Project Team, F4E, Rokkasho Fusion Institute, Japan*

[b] *Fusion Energy Research and Development Directorate, QST, Rokkasho Fusion Institute, Japan*

* Corresponding author.

E-mail address: juan.knaster@ifmif.org (J. Knaster).

[1] Present address: Facility for Rare Isotope Beams (FRIB), Michigan State University, East Lansing, MI, USA.

Abstract

The flowing lithium target of a Li(d,xn) fusion relevant neutron source must evacuate the deuteron beam power and generate in a stable manner a flux of neutrons with a broad peak at 14 MeV capable to cause similar phenomena as would undergo the structural materials of plasma facing components of a DEMO like reactors. Whereas the physics of the beam-target interaction are understood and the stability of the lithium screen flowing at the nominal conditions of IFMIF (25 mm thick screen with +/–1 mm surface amplitudes flowing at 15 m/s and 523 K) has been demonstrated, a conclusive assessment of the evaporation and condensation of lithium during operation was missing. First attempts to determine evaporation rates started by Hertz in 1882 and have since been subject of continuous efforts driven by its practical importance; however intense surface evaporation is essentially a non-equilibrium process with its inherent theoretical difficulties. Hertz-Knudsen-Langmuir (HKL) equation with Schrage's 'accommodation factor' $\eta = 1.66$ provide excellent agreement with experiments for weak

http://dx.doi.org/10.1016/j.heliyon.2016.e00199

evaporation under certain conditions, which are present during a Li(d,xn) facility operation. An assessment of the impact under the known operational conditions for IFMIF (574 K and 10^{-3}Pa on the free surface), with the sticking probability of 1 inherent to a hot lithium gas contained in room temperature steel walls, is carried out. An explanation of the main physical concepts to adequately place needed assumptions is included.

Keywords: Energy, Materials science, Nuclear physics, Physics methods, Plasma physics

1. Introduction

The endeavours towards making a fusion relevant neutron source available for fusion materials qualification (and development), a decades old pending indispensable step of world nuclear fusion community, is coming to an end. In future fusion power plants, the reactor vessel's first wall will be exposed to neutron fluxes in the order of 10^{18} $m^{-2}s^{-1}$ with an energy of 14.1 MeV causing potentially >15 dpa_{NRT} per year of operation [1, 2]. The plasma facing components shall withstand the severe irradiation conditions without significant degradation for a period long enough to make a power plant viable and economically interesting. ITER, with its estimated maximum of 3 dpa of irradiation exposure at the end of its operational life, does not need the results from a fusion relevant neutron source for its licensing. However, in future fusion reactors, this neutron damage will be reached within few months of operation. Thus, an understanding of the degradation of the mechanical properties of the structural materials exposed to the DT nuclear reactions will be soon indispensable to design next generation of fusion reactors.

The accumulation of gas in the materials microstructure is intimately related with the colliding neutron energy. In steels through $^{54}Fe(n,\alpha)^{51}Cr$ and $^{54}Fe(n,p)^{54}Mn$ reactions, which are responsible for most of the α-particles and protons produced. These reactions exhibit incident neutron energy thresholds at around 3 MeV and 1 MeV respectively. Therefore fission neutron sources, which show an average energy around 1–2 MeV as per Watt's distribution spectrum, cannot adequately suit the testing requirements for fusion materials since the transmuted He production rates are far from fusion reactor's (actually around 0.3 appm He/dpa compared with around 10 appm He/dpa for 14 MeV neutrons) [3]. In turn, spallation sources produce a neutron spectrum with long tails reaching the typically GeV order of the incident particle energy. These neutron energies generate light ions as transmutation products, which induce measurable changes of material properties (driven by changes of few ppm and about one order of magnitude higher appm He/dpa than fusion neutrons [4, 5]).

http://dx.doi.org/10.1016/j.heliyon.2016.e00199

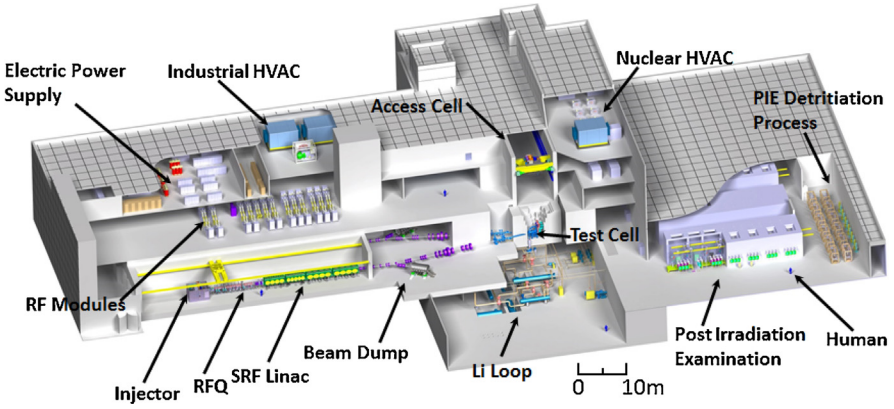

Fig. 1. Artistic bird's eye view of the IFMIF's Main Building [6].

IFMIF (see Fig. 1), the International Fusion Materials Irradiation Facility, is presently under its Engineering Validation and Engineering Design Activities (EVEDA) phase under the frame of the Broader Approach Agreement between Japan and EURATOM. IFMIF/EVEDA entered into force on June 2007 with the mandate to produce an integrated engineering design of IFMIF and the data necessary for future decisions on the construction, operation, exploitation and decommissioning of IFMIF, and to validate continuous and stable operation of each IFMIF sub-system [6].

The successful accomplishment of the Engineering Design Activities (EDA) phase [7], together with the on-going success of the Engineering Validation Activities (EVA) phase [8, 9, 10], where only remains the accelerator facility to be validated, whose installation and commissioning in Rokkasho is advancing [11], has allowed to taking decisions on the construction of a fusion relevant neutron source. A facility capable to provide 14 MeV neutrons and the needed flux will be likely available by the middle of next decade, to timely characterize materials in compliance with fusion roadmaps.

Neutrons will be generated primarily by deuteron Li(d,xn) stripping reactions [12], with a broad peak at 14 MeV thanks a 40 MeV deuteron beam at 125 mA in CW (100% duty cycle) and shaped on a 200 mm x 50 mm beam footprint colliding with a flowing liquid lithium target. The suitable flux of neutrons will irradiate 12 capsules containing above 1000 small specimens that will characterize mechanically 24 sets of materials at 12 different chosen temperatures ranging between 523 K and 823 K. Fig. 2 shows the seminal concept [17]; the design has matured throughout decades of worldwide development [13, 14, 15, 16]. Today's technological maturity is thanks to the EVEDA's successful validation activities [8, 9, 10], however the concept remains valid.

http://dx.doi.org/10.1016/j.heliyon.2016.e00199

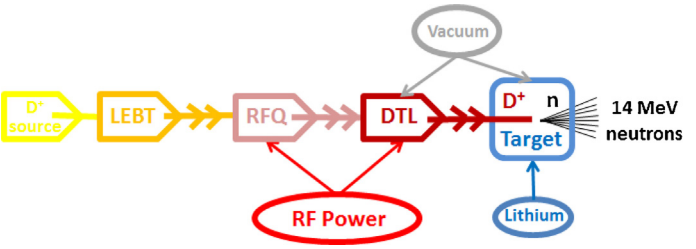

Fig. 2. Principle of a Li(d,xn) neutron source as proposed for FMIT with a Low Energy Beam Transport (LEBT) line, its Radio Frequency Quadrupole (RFQ), its Drift Tube Linac (DTL) and the Lithium Target impacted by the D^+ beam to generate the 14 MeV neutrons. More details of these accelerator components and their evolution framed by Fusion materials research can be found in [55, 56].

2. Background

The lithium screen serving as beam target presents two main functions: 1) react with the deuterons to generate a stable neutron flux in the forward direction and 2) dissipate the beam power in a continuous manner [18].

The impossibility for any known material to be directly bombarded by such high deuteron fluence constrains the lithium jet to operate with a free surface matching the beam footprint exposed to the vacuum conditions present in the beam line. Furthermore, the jet must also be thick enough to completely absorb the deuteron beam, but also to maximize the neutron flux and available high flux tested volume; thus the jet and its guiding structural backwall plate must be kept as thin as possible. The distance of the High Flux Test Module to the target backwall has a strong influence on the neutron flux available for material testing; actually calculations show around 1% reduction per mm increased distance [19]. The feasibility of the yearly remote removal of the backwall plate, without welding thanks to the bayonet concept [20], allows the fixation of the required tight tolerances.

The design of the Target Facility of IFMIF has already been described [7, 21]. Its layout, integrated in full IFMIF plant is visible in Fig. 3.

2.1. The validation of the Target Facility of IFMIF

To validate the operational conditions of IFMIF's Target Facility, a lithium loop was constructed in the JAEA premises of Oarai as one of the validation activities under EVEDA phase [8], the EVEDA Lithium Test Loop (ELTL), which started its operation in March 2011 [22]. Unfortunately, the Great East Japan Earthquake damaged the ELTL just few days after its successful commissioning; thus the operation was suspended for 16 months to allow for a careful inspection and repair. The validation phase could only re-start in September 2012 with severe limitations

http://dx.doi.org/10.1016/j.heliyon.2016.e00199

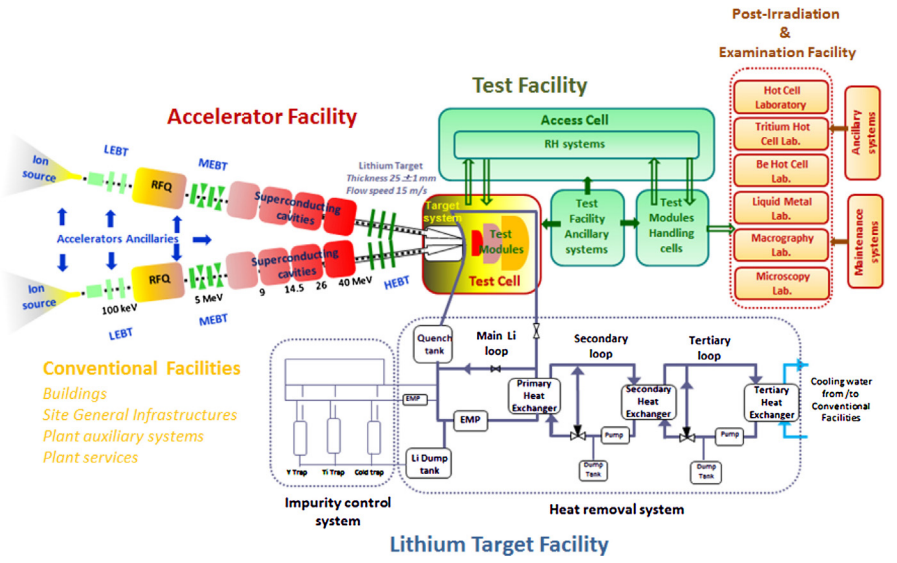

Fig. 3. Layout of IFMIF Facility including the Target Facility [54].

in the operational time and available budget. The ELTL is the largest world lithium loop to date.

The ELTL main objective was the demonstration that the flow operational conditions of IFMIF's Target Facility are achievable. These challenging operational conditions are the long term continuous operation with the simultaneous fulfilment of: 1) 15 m/s flow, 2) 250 °C, 3) 10^{-3} Pa vacuum exposure to beam line, 4) within +/–1 mm amplitude of free surface wave [7]. The lithium inventory of the ELTL of 5 m^3 compared with the planned 9 m^3 of IFMIF allowed to accommodate the 25 mm thick beam target but with 100 mm vs the designed 260 mm of IFMIF to overcome capillary driven edge effects and ensure a flat lithium free surface facing the beam 200 × 50 mm deuteron beam footprint.

The appearance of cavitation phenomena during initial stages of operation under vacuum, and precautions against potential cavitation pitting, led to explore the dependence of the free surface thickness with pressure by exposing the jet to all decades from 10^{-3} Pa to 10^5 Pa without observable thickness variation [23]. This ensured the validity of performing the long term operation under Ar atmosphere at 10^5 Pa with no cavitation. The on-line monitoring was possible by means of an interferometry approach laser-based distance meter, specifically developed under IFMIF/EVEDA framework [24]. This allowed the assessment of the specified thickness variation of ±1 mm with a resolution and precision within <0.1 mm. Nevertheless, its integration in the design of the Target Facility of IFMIF was not included in the Engineering Design of IFMIF [7], since it will possibly demand further development related with its radiation hardness.

http://dx.doi.org/10.1016/j.heliyon.2016.e00199

Efforts to understand the unexpected cavitation phenomena observed were implemented as part of the engineering validation tasks to prevent the appearance of such phenomena in the Target Facility of IFMIF. After impingement, possibly due to a slight uncorrected misalignment following the earthquake, there was a partial backward flow in the outlet 60° elbow, thus droplet formation, and hence free surface increase with lithium vapour production (in the order of 0.1% to 0.2% vapour fraction according to simulations). Such vapour is therefore ready to be captured and reintroduced in the main flow. As the static pressure is recovered due to impact, bubble collapses and cavitation takes place. CFD simulations and careful measurements coincided within 30 mm in the prediction of the location of cavitation source [23].

The long term stable operation of a lithium flow with the nominal conditions of IFMIF was successfully demonstrated thanks to the 1302 h operation at the nominal velocity of 15 m/s, of which 571 h were achieved during 25 consecutive days with 12 measurements spanned in time of the full width every 5 mm, with the perfect match of all measurements visible in Fig. 4 [10].

2.2. The beam – target interaction of IFMIF

The beam – target interaction was subject of a careful theoretical study for FMIT reaching analytical expressions for the maximum possible perturbances induced by beam momentum transfer or density gradients [25, 26]. Safe results were obtained for FMIT in presence of beam power density x10 higher than the 1 GW/m^2 of IFMIF (driven by the smaller beam footprint). In IFMIF, the heat is evacuated with the liquid lithium, which flows at a temperature of 523 K with a nominal speed of

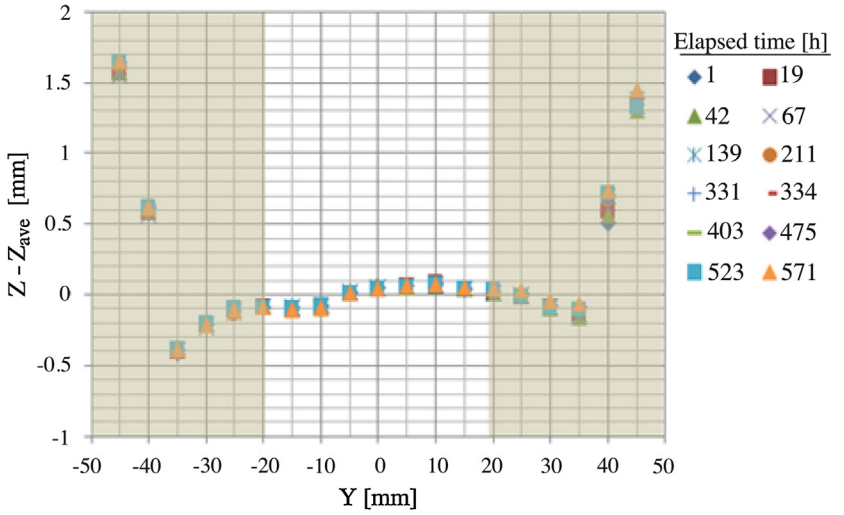

Fig. 4. Average thicknesses of lithium flow during the 25 days that in continuous manner was in operation with 12 measurements (all overlapped) spanned in 571 h.

http://dx.doi.org/10.1016/j.heliyon.2016.e00199

15 m/s exposing its surface to the accelerator high vacuum. The average temperature rise in the liquid is only about 50 K due to the cross flow and its short exposure of 3.3 ms to the two concurrent 5 MW deuteron beams and high heat capacity of lithium. The heat removal system of the main lithium loop circulates the 97.5 l/s lithium flow from the exit of the beam target to a 1.2 m^3 quench tank, where it is slowed down and thermally homogenized before it flows to the electromagnetic pump. The lithium is then cooled to 523 K by a serial of heat exchangers [7, 21]. The temperature reached during operation in the lithium surface exposed to the accelerator beam vacuum is 574 K [18] as shown in Fig. 5.

The flowing lithium is shaped and accelerated in proximity of the beam interaction region by a two-stage reducer nozzle to form the concave jet of 25 mm thickness channelled by the backwall with its R250 mm in the beam footprint area. This concave shape and the high speed of flowing lithium builds a centrifugal acceleration of 90 g; this compression raises the boiling point of the flowing lithium guaranteeing stable liquid phase in Bragg's maximum heat absorption regions [18].

Despite the efforts in IFMIF not to enter into over-saturation scenarios, recent experiments framed by the Facility for Rare Isotope Beams (FRIB) have demonstrated that over-saturation scenarios are safe. A 4.6 mA proton beam at 65 kV, with a beam Gaussian size $\sigma = 0.7$ mm, colliding on a lithium jet, confirmed the severe super saturation conditions that lithium can hold without

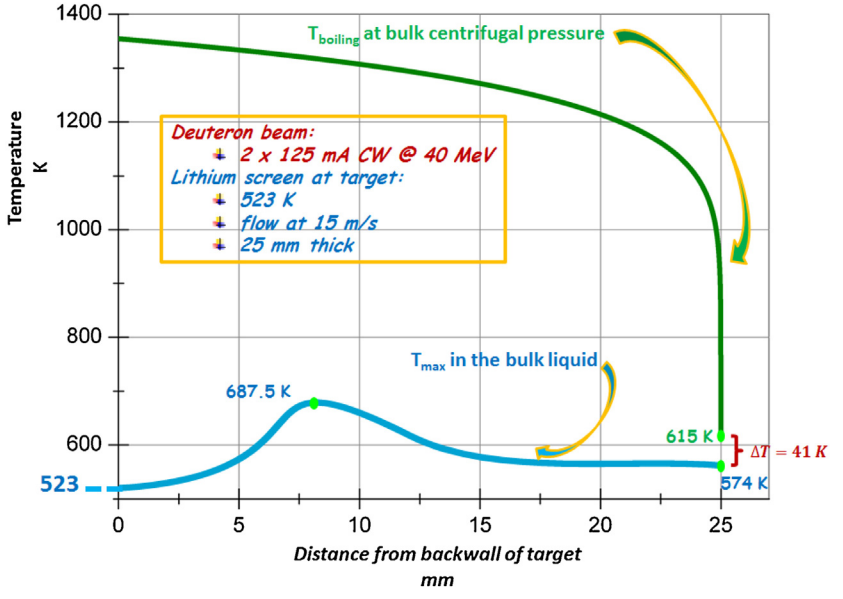

Fig. 5. Tmax envelope in the beam footprint under nominal conditions at different depths (in blue) vs Ts corresponding to the centrifugal pressure in the flowing lithium (in green). 615 K corresponds to the beam line pressure of 0.001 Pa [18].

http://dx.doi.org/10.1016/j.heliyon.2016.e00199

nucleation [27]. This is an expected behaviour due to the high surface tension of liquid lithium. The proton beam collided in a 14 mm wide and 10 μm thick lithium screen flowing at 50 m/s; the Bragg peak being of <2 μm thick released a power density of $>10^3$ times higher than the 150 kW/cm^3 power densities of IFMIF in Bragg peak regions. This success has validated the concept of free flowing lithium as stripper of uranium beams, capable of sustaining without instabilities more than twice the FRIB's expected maximum volume power density deposition. It is to be stressed that this observation is theoretically backed with the simple analysis of the minimum radius to balance the force of a vapour bubble growth

$$P_v - P_l = \frac{2\sigma}{r} \tag{1}$$

yielding r of ~2 mm for 1000 K but >1 m for 523 K flowing lithium operational temperatures.

2.3. The vaporisation phenomena of a Li(d,xn) neutron source

Careful tests to determine the vaporization phenomena from the lithium screen have been carried out in three occasions during last three decades, allowing a mature understanding of the phenomena to be expected.

In the early 80s, a prototype of the Target Facility of FMIT with its 3.8 m^3 of lithium and 543 K flowing temperature, the Experimental Lithium System (ELS), was constructed to validate the technological feasibility of FMIT concept [28]. Many lessons learnt were implemented and improved in the ELTL [29]. In what concerns the vaporization phenomena, subject of the present paper, the appearance of frost led to a thorough experimental campaign to understand it. The presence of potassium and sodium as impurities in commercial lithium, and their physico-chemical affinity as alkali metals led to their detection in non-negligible quantities in the frost observed.

A Φ120 mm (as FMIT's accelerator beam pipe would have been) and 5 m long projected from the target structure was installed in the second generation target Mark II (see Fig. 6), the flowing lithium exposed to pressure and vacuum and vaporization rates from the lithium jet and deposition rates along the tube were determined. A temperature gradient (from 673 K to RT) was achieved by means of heaters installed along the tube to simulate the estimated beam pipe operational temperatures. This configuration provided interesting observations to occur during operation of a future Li(d,xn) fusion relevant neutron source.

The dependence of the sticking factor with the beam tube temperature was confirmed: if the temperature of the simulated beam pipe was below the vapour saturation temperature at the beam pipe pressure, then the sticking factor $\alpha = 1$

http://dx.doi.org/10.1016/j.heliyon.2016.e00199

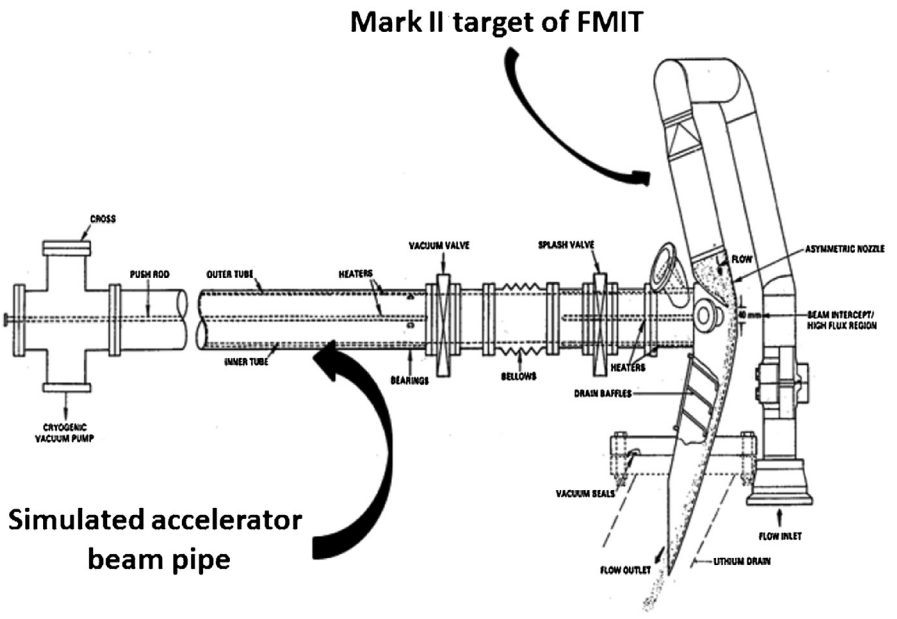

Fig. 6. Simulated accelerator beam tube attached to the second generation target Mark II for vaporization measurements during FMIT programme.

(actually, the deposition started from the point where the beam pipe presented temperatures below such a point). This was always the case for lithium; however for sodium there was a crossing at about 1 m upstream the simulated beam pipe. In turn, for potassium the beam pipe temperature was always above the saturation temperature, implying potentially a low sticking factor; however, its deposition started in a correlated way with sodium. This last point was attributed to the formation of NaK, which exhibits lower vapour pressure than sodium or potassium, thus it deposits faster.

Another remarkable point observed was that, while under vacuum the deposition grew following a parabolic behaviour, in turn, under pressure the deposition was linear along the simulated beam pipe. The mean free path of a molecule follows

$$l = \frac{K_B T}{\sqrt{2}\pi\sigma^2 P} \tag{2}$$

where σ is effective cross sectional area for spherical particles with radius r and P the pressure. Thus, the observed behaviour was found reasonable since under vacuum conditions, the mean free path of a molecule is in the order of meters; therefore a molecule evaporated will impact the target frame or even the beam pipe wall close to the lithium free surface before colliding with other molecules. However, under atmospheric pressure conditions, with mean free paths l in the order of μm, the molecules can be easily convected upstream before colliding with the beam pipe walls.

http://dx.doi.org/10.1016/j.heliyon.2016.e00199

It is worth stressing that the deposition of lithium is not impacted by the beam pipe temperature since it exhibits T_s below possible beam pipe wall temperatures and in extreme high vacuum (XHV) operational regions. In addition, as expected, the vaporization measured under pressure conditions was lower than under vacuum, one of the reasons being that the flowing lithium behaves as an active pump reducing the pressure in the regions close to the jet surface.

The vaporization measurements in the ELS showed 1.34 mg/cm^2·day for lithium. The values measured were almost a factor x10 from the estimated values. Remarkably sodium deposition was measured about a factor x4 higher than those measured for lithium. It is to be noted that the composition of the lithium used in the ELS presented a purity of lithium of 99.7% with 0.22% of Na and 0.0005% of potassium.

The LTF-M is the second and smaller loop (with 270 l of lithium and capable to reach 20 m/s of flow speed in the target region) that was constructed framed by a Li (d,xn) technological efforts. Under ISTC programme, early 00s in Obninsk this lithium loop was constructed to perform additional validation activities [30]. In what regards, the tests related with vaporization of liquid lithium, the results were controversial due to the appearance of droplets driven by a poorly controlled flow. Undesired variations in the jet temperature between 257−280 °C during the 238.5 h that the vaporization tests were in place; this lead to controversial results. A deposition of 8.7 mg/cm^2·day was measured; this meant about x6 higher deposition rates than the ones observed in FMIT's ELS.

It is to be noted that the measurements for the LTF-M in what concerns potassium and sodium (which are not so strongly impacted by the droplets given their relatively poor presence) correlated nicely with values anticipated by the analysis [30].

Additional more careful vaporization experiments have been recently performed in the ELTL under IFMIF/EVEDA frame with the exposure of the 15 m/s at 523 K flowing lithium to the nominal vacuum values. These results are conclusive, however are not yet published by the time of drafting this article [31].

3. Theory

Evaporation, condensation and adsorption are linked phenomena but ruled with different physics as was already described by Langmuir back in 1932 [32]. Not only evaporation and condensation are wrongly frequently perceived as equivalent, but the concept of adsorption is often misunderstood with wrong descriptions even present in scientific articles where the word 'absorption' is misleadingly used for adsorption phenomena. Adsorption accounts for the temporary permanence of a gas molecule in the surface of solids upon their impact whereas absorption implies

 http://dx.doi.org/10.1016/j.heliyon.2016.e00199

penetration of molecules in the substrate bulk material typically following Fick's law of diffusion.

3.1. Evaporation and condensation

Evaporation and condensation are an interfacial molecular transport problem, which surprisingly is not yet well understood, despite its ubiquity, practical relevance and time passed since the first model was proposed. These processes involve either molecules escaping from a liquid surface or an incident vapour molecule being captured by it. Under equilibrium conditions, the number of molecules evaporated and those condensed are equal; furthermore, the liquid and vapour temperatures are uniform, since otherwise there would be a positive flow of heat.

Following a classical Kinetic Theory approach, the first attempt to explain the evaporation phenomenon in 1882 by Hertz [33], developed by Knudsen in 1915 [34] and by Langmuir 1916, who extended the comprehension to solids [35], resulted in the 100 years old Hertz-Knudsen-Langmuir (HKL) model (or just Hertz-Knudsen depending on the author's taste). Unfortunately, it yields results mismatching the measurements.

Direct observation of the interface does not show other than an abrupt change in the uniform properties of the two phases (liquid vs gas); the discrepancies between theory and observations were often attributed to the inaccuracy of data retrieved. Undoubtedly, a key factor is the difficulty on carrying out efficiently experiments, where the following essential requirements have often been disregarded: 1) an accurate estimate of the surface temperature of the evaporating substance, 2) a precise knowledge of the interfacial area, 3) a surface which will condense all the evaporating molecules without reflecting, 4) distance between vaporizing surface and condensing surfaces small with respect to the mean free path and 5) control of splashes and droplets if non-stagnant (when tests with liquids this becomes a critical factor). However, the complex transport phenomena present in the thin liquid-gas interfacing Knudsen layer, where a gas dynamics discontinuity takes place, are the driver of the discrepancies. Knudsen tried to overcome the divergences with the inclusion of the evaporation coefficient [34]

$$\alpha_e = \frac{experimental \quad rate \quad of \; evaporation}{Maximum \quad theoretical \quad rate \quad of \quad evaporation}$$

presenting for water at low pressures a wide range of quoted values in the literature (from 0.01 to 1 for the undoubtedly best studied liquid) [36]; making visible the incompleteness of the understanding. To overcome the frustration, the conclusion from Hertz in his seminal work from 1882 was that his expression would define the maximum possible rate of evaporation, which depends only on the temperature of surface and nature of the substance (the existence of such a maximum had been

http://dx.doi.org/10.1016/j.heliyon.2016.e00199

anticipated by Stefan in 1873 [37]). This hypothesis is confirmed today, since this evaporation rate is limited by the sound speed of the gas molecules [38]. Thus, this maximum possible evaporation rate $\dot{m}_H$ per unit surface would be given by Hertz's original expression

$$\dot{m}_H = P\sqrt{\frac{M}{2\pi RT}} \tag{3}$$

where R is the universal gas constant, M is the molecular mass; T is the absolute temperature of the liquid and P the vapour pressure at such temperature.

The evaporation and condensation coefficients may be equal for some simple liquids; however such equality disappears under conditions removed from equilibrium given that the evaporation and condensation phenomena depend on different variables (for a careful assessment see [39]). Luckily, the prediction for liquid metals, which evaporate mostly monoatomically, seem to work better with α_e usually close to unity [40], and with close to ideal gas behaviour of metals vapours. Two variables might though cause a slower evaporation rate of a liquid metal than the predicted by the theory: 1) surface temperature and 2) accumulation of impurities in the surface. It is to be stressed that the liquid surface temperature is lowered due to the heat losses from the surface and the endothermicity of evaporation phenomena, with a reduction of the vapour pressure. However, in case of non-stagnant liquids the impact of both factors is obviously reduced.

The HKL develops Hertz's seminal proposal introducing the evaporation/condensation coefficients, basically to adapt retroactively estimations with observations of particular experiments, but thus with limited success to anticipate results [41].

$$\dot{m}_{HKL} = \sqrt{\frac{M}{2\pi R}}\cdot\left(\alpha_c\frac{P_v}{\sqrt{T_v}} - \alpha_e\frac{P_l}{\sqrt{T_l}}\right) \tag{4}$$

where P_l is the saturation pressure of the liquid at T_l, P_v and T_l the pressure and temperature of the vapour above Knudsen layer and α_c the condensation coefficient.

This widely used simple model results from the wrong assumption that at the evaporating surface the vapour particles follow a half-Maxwellian distribution function, what intrinsically implies that the evaporation is an expansion of unbound non-interacting particles, thus the depth of the potential well at the boundary between the condensed and gaseous phases is assumed to be zero. Schrage developed further this model, implementing continuum mechanics principles in the off-equilibrium Knudsen layer discontinuity, with the inclusion of a new coefficient, which he called 'accommodation factor' η, that yielded double HKL

http://dx.doi.org/10.1016/j.heliyon.2016.e00199

evaporation model results when $\alpha_e = \alpha_c = 1$ [42]. However, the incomplete approximation that the Knudsen layer would be an isolated system [43] lead to the remaining unsatisfactory anticipation of experimental results.

In fact, all efforts based on HKL model refinements can only be unsuccessful since contradict the more accurate nowadays model of condensed matter as a collection of particles that are bound to each other resting within potential wells. The efforts to overcome this flaw are maturing with the novel Statistical Rate Theory [44] based on quantum and statistical mechanics, still in process of further development. However, its complexity and insufficient completeness will likely prevent wide utilization for practical purposes. Remarkable are the recent results obtained by Semak with a novel approach combining statistical mechanics, gas dynamics and thermodynamics that has allowed an accurate theoretical prediction of the saturation vapour pressure dependence on temperature for lithium [45].

Safaranian has reviewed the results available in the literature [38] related with vaporization phenomena for liquid metals showing a nice correlation for weak evaporation with HKL formula. We will follow his conclusion in our assessment of evaporation of Li(d,xn) neutron sources from free flowing lithium exposed to vacuum of Section 4, including the apparent evaporation coefficient $\eta = 1.66$, what we can also consider it to be a modern refinement of Schrage's 'accommodation factor' $\eta = 2$.

$$\dot{m}_H = 1.66P\sqrt{\frac{M}{2\pi RT}} \tag{5}$$

It is to be remarked that this factor has been theoretically estimated by various authors [40, 46, 47, 48], as Safaranian explains, becoming the most accepted value for the weak evaporation phenomena of liquid metals.

3.2. Adsorption

Back in 1913, Langmuir discovered that atoms of metal vapours, striking a clean and dry glass surface in high vacuum, were immediately condensed as solids at the first collision with the surface. He concluded that when gas molecules strike a surface, the majority of them did not rebound by elastic collisions, but were held in the surface by cohesive forces [35]. On the other hand, according to the condensation-evaporation theory, there is no direct connection between the condensation and subsequent potential evaporation of a molecule; they are independent phenomena.

The adsorption of gases or vapours (understood as a gas whose molecules gained energy and vaporized from a substance which at room temperature is either a solid or liquid) on solids is due to the time lag between the 'condensation' and the 'evaporation' of the molecules from the surface. Atoms striking a surface, if not

http://dx.doi.org/10.1016/j.heliyon.2016.e00199

trapped, have a certain sojourn time before desorption, depending on the temperature of the surface and the intensity of the forces holding the atom. Trapping and sticking are close phenomena, but when sticking the impinging molecule does not lose sufficient energy as to prevent its desorption induced by the thermal vibration of the substrate surface atoms. They may remain 'sticked' in the available adsorption vacancy sites physisorbed by Van der Waals forces [49].

Langmuir's approach assumed no interaction between adsorbed molecules, this incomplete model was overcome 1938 by Brunauer, Emmett and Teller [50], the BET model, for multilayers scenario with typically sticking factors, α, of 1 also through Van der Waals forces between the molecules themselves, leading to a potentially infinite number of overlapping layers. Let us stress that it might also happen that adsorption is accompanied by absorption, if the adsorbed species penetrate into the solid, governed by Fick's diffusion law.There were not much advancements in the understanding of trapping/sticking phenomena until the development by middle 60s of vacuum technology induced by growing particle accelerators performances, and Aerospatiale research that demanded ultra-high vacuum lab conditions. These new possible experimental conditions with extremely low pressures allowed direct observation on atomically clean surfaces.

From the kinetic theory of gases, the flux of molecules impinging a surface exposed to a gas of certain pressure and temperature is given by

$$\Phi = \frac{P}{\sqrt{2\pi m K_B T}} \tag{6}$$

where P is the gas pressure, m the molecular mass, K_B the Boltzmann's constant and T is the absolute temperature, which can in turn be simplified in

$$\Phi = \frac{\rho \cdot v}{4} \tag{7}$$

where ρ the number density, and v is the molecule speed described by

$$v = \sqrt{\frac{8K_B T}{\pi m}} \tag{8}$$

The controversial unit in surface materials studies called *Langmuir* equals the number of molecules that would impinge per cm^2 of surface under 10^{-6} torr in a second (thus, its units are *torr·s*). However, as per Eqs. (6) and (7), this number of molecules would be different depending on the gas nature and temperature. In turn, the exact number of possible sticked molecules to form a monolayer depends mainly on the nature of the substrate, but it is typically $\sim 10^{15}$ molecules/cm^2.

 http://dx.doi.org/10.1016/j.heliyon.2016.e00199

4. Results and discussions

Conservative estimations of the vaporization rates assuming a window free surface exposure as the beam footprint and temperature of the free surface were estimated in <1 g/year for FMIT [25] and of 6.5 g/year for IFMIF [30]; both results are equivalent considering the increased free surface of IFMIF. The calculation methodology for those estimated vaporization rates of FMIT is not reported. Unfortunately, the flaws in the experimental efforts carried out in the 80s [28] carefully detailed in Section 2.3 'The vaporisation phenomena of a Li(d,xn) neutron source' did not allow the validation of these analytical estimations for liquid lithium. This lead to new unsuccessful attempts in the 00s with the ISTC's LTF-M, where HKL theory with an accommodation factor of 1.66 was used but not validated with experiments in what concerns the vaporization of lithium, probably due to appearance of droplets (see Section 2.3 for an explanation). This has led to the repetition of vaporization tests under IFMIF/EVEDA in its ELTL facility [31].

A recalculation using HKL simplified formula corrected by an accommodation factor of 1.66, which is the most widely accepted value in today's models for weak evaporation phenomena, is available in Table 1.

This approach has been also applied for estimating the vaporization rates of ELTL, which have been realized 1) in a canonical way taking into account historical difficulties for adequate experimentation and overcoming flaws in former experiments related with a Li(d,xn) in ELS during FMIT times [28] and LTF-M in Obninsk last decade [30], and 2) with a scientific accurate estimation of the vaporization from precise measurement of the deposited lithium in exposed samples. The results of the measurements in the ELTL are not yet published by the time of publication of this paper [31], but given the optimal experimental setup, a

Table 1. Calculation of vaporization rates of ELTL and IFMIF and total estimated for IFMIF using the HKL formulation with an accommodation factor $\eta = 1.66$.

	Li Temp ***K***	**Target Free surface** ***mm*^{2}**	**Li$_{vap}$/cm^2 per day** ***g·cm*$^{-2}$**	**Total Li$_{vap}$ per year*** ***G***
ELTL	523	100 × 400	0.0373×10^{-3}	–
IFMIF	574**	260 × 400	0.806×10^{-3}	76.7***

* Assuming the specified 70% availability of the facility.

** Lithium flowing temperature of IFMIF is 523 K, however this is the maximum temperature reached in the free surface after beam impact as shown in Fig. 5.

*** This value conservatively assumes that an area of 260 × 230 mm^2 exhibits a uniform temperature of 574 K and 260 × 170 mm^2 above the beam footprint a uniform temperature of 523 K.

http://dx.doi.org/10.1016/j.heliyon.2016.e00199

close result with the calculations here included is expected, thus providing soundness to this estimation for IFMIF [6, 7].

Alkaline metal impurities in flowing lithium can also lead to vaporization; this was observed in both ELS and LTF-M. The reason for this becomes obvious in Table 2 below, where fusion and melting temperature of lithium, sodium and potassium are provided. This liquid state range (lower melting temperature and substantially lower bowling temperature) yields higher vapour pressures if compared with lithium at Li(d,xn) operational temperatures, that in turn leads to significantly higher vaporization rates despite their marginal presence as impurities in commercial lithium.

Thus, in the future construction phase of a Li(d,xn) fusion relevant neutron source, special care shall be taken to specify minimum possible sodium and potassium impurities. Assuming these are limited to 10 wppm, few tens of grams will be present in the 9 m^3 of IFMIF, which would likely be fully evaporated in few months of operation.

The sticking factor of vaporized lithium molecules in room temperature stainless steel surfaces is basically 1; this makes impossible the potential arrival of lithium gas molecules to the superconducting equipment. The superconducting accelerating cavities are placed more than 30 m from the beam – lithium target interface region, with a bent trajectory of 9° and significant conductance reduction in beam pipes when approaching the cryogenic beam accelerating equipment (see Fig. 7).

A concern could possibly be aerosol formation which potentially enhances vaporization. An aerosol is a gas, which presents in suspension solid particles or liquid micro-drops condensed. However, the vapour to condense without nucleation inducers must be supersaturated (its partial pressure must be greater than its vapour pressure). This can happen due to three reasons: 1) the vapour pressure is lowered by lowering the temperature of the vapour, 2) chemical reactions that either increase the partial pressure of a gas, or lower its vapour pressure or 3) the addition of another vapour that lowers the equilibrium vapour pressure following Raoult's law on volatile solved in liquids. Therefore, aerosols is not a concern since none of the three conditions aforementioned for its formation can occur [18].

Table 2. Fusion temperature (T_f) and boiling temperature (T_b) of alkaline metals.

Element	**Lithium Li**	**Sodium Na**	**Potassium K**
T_f [K]	453.5	370.7	336.4
T_b [K]	1615	1156	1032

http://dx.doi.org/10.1016/j.heliyon.2016.e00199

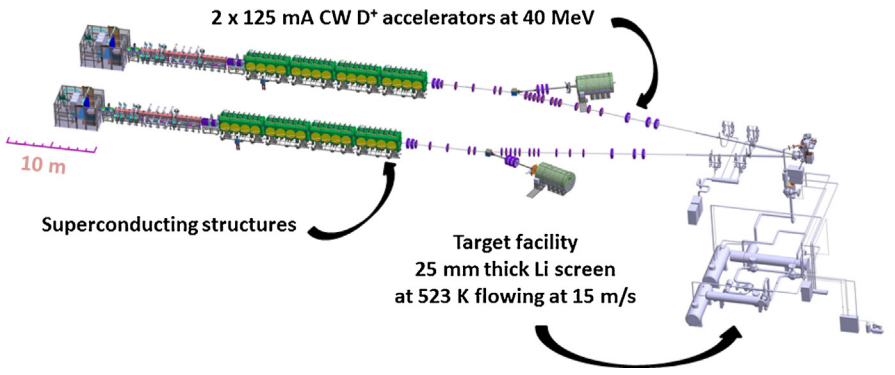

Fig. 7. Layout of IFMIF where it is visible the angle of 9° in the accelerator layout to avoid neutron backscattered to the superconducting cavities.

Conclusive thermohydraulic analysis of the lithium flow of a Li(d,xn) neutron source with one only 125 mA CW 40 MeV deuteron accelerator and a beam footprint of 200 × 50 mm^2 colliding on a 15 m/s flowing lithium at 523 K, as DONES [51] or A-FSN [52] could exhibit, is presently missing. It is obvious that the halved beam power will lead to <574 K than those that IFMIF will reach in its free surface (see Fig. 5). The lower it is, the lower the corresponding vapour pressure and thus reduced vaporization rate. Therefore, the value of 76.7 g of total vaporized lithium per year of operation of IFMIF, assuming the 70% target specified facility availability, is a conservative value usable for a future simplified Li(d,xn) fusion relevant neutron source with one only deuteron accelerator line [51, 52].

5. Conclusions

Vaporization of lithium during IFMIF operation, and the ensuing adsorption in the accelerator beam pipe stainless steel walls, will take place during the facility operation due to the necessary exposure to vacuum conditions of the 523 K flowing lithium being impacted by the 200 × 50 mm^2 footprint deuteron beam. The 2 × 5 MW beam power absorbed by the 25 mm thick and 15 m/s speed lithium screen will lead to 574 K maximum temperature in the lithium free surface. Assuming the specified 10^{-3} Pa pressure and, conservatively, a uniform temperature in its 260 × 230 mm^2 open surface channelled downstream by the backplate, an amount of 76.7 g of lithium vaporized per year of operation is estimated through the HKL equation with an 'accomodation factor' $\eta = 1.66$. This Eq. (5) is also used to estimate the vaporization in the ELTL during the IFMIF/EVEDA phase, where careful measurements have been carried out overcoming the controversial available results from ELS lithium target experiments during FMIT times in the 80s [28], and last decade's LTF-M in Obninsk [30] under ISTC programme. These results are published elsewhere [31].

http://dx.doi.org/10.1016/j.heliyon.2016.e00199

The sticking factor of the hot vaporized lithium will be of 1 in the stainless steel accelerator beam pipe, thus lithium molecules will be adsorbed along the >3 m long beam pipes traversing the test cell shielding wall. Thus, the adsorbed vaporized lithium will form some μm thin coating formed by few 10^4 monolayers in the several m^2 stainless steel exposed substrate surface.

In this assessment, the influence of the deuteron beam potentially jeopardizing the lithium vaporization has been neglected. However, the impacting footprint of 200 × 50 mm^2 deuteron beam, with basically no deuteron reflection expected (Bragg peak of 40 MeV deuterons in lithium is 19 mm) will transfer its unidirectional momentum to the target, what should induce a static pressure on the lithium surface exposed to vacuum, and hence reducing the estimated vaporization rate reported in Table 1, where an exposure to the specified operational vacuum of 10^{-3} Pa was considered. Assuming an ideal gas behaviour, in thermal equilibrium and isotropical momentum distribution, Eq. (6) applies yielding 47 Pa of pressure on the lithium target; however, possibly more adequate would be, given the unidirectional momentum of deuterons, to estimate this induced static pressure by

$$P = m_d v_d \phi_d \tag{9}$$

that would, in turn, yield 32 Pa. Last but not least, tests carried out in Rare Isotope Accelerator project in the US with an electron beam 1 MeV with 20 kW beam power and up to 25.5 GW/m^2 power density (compared with the 1 GW/m^2 in the lithium target of IFMIF) being absorbed by a free flowing lithium screen, allowed the observation of an increase of the pressure in the proximity of the target to values in the order of 10^{-2} Pa, which could not be due to an enhanced vaporization of the free surface but originated by ion induced desorption from the beam line walls [53].

In conclusion, whereas the long term stability of the lithium flow under the specified challenging conditions (25 mm thick screen with +/–1 mm surface amplitudes flowing at 15 m/s and 523 K) has been demonstrated in the EVEDA Lithium Test Loop [10], and the impact of the 2 × 5 MW deuteron beam power has been shown as incapable to perturb this long term stability [18], the vaporization of lithium during operation is difficult to anticipate. In any case, the 76.7 g potentially vaporized per year of operation and adsorbed in the >3 m long accelerator stainless steel beam pipe traversing the Test Cell shielding wall forming a thin coating of few μm, can be considered the maximum possible value of lithium vaporized and its consequences.

In the case that a simplified version of IFMIF is constructed with one only deuteron accelerator 125 mA CW at 40 MeV [51, 52], the maximum annual vaporization will always be smaller than the 76.7 g here reported.

 http://dx.doi.org/10.1016/j.heliyon.2016.e00199

Declarations

Author contribution statement

Juan Knaster: Analyzed and interpreted the data; Contributed reagents, materials, analysis tools or data; Wrote the paper.

Takuji Kanemura: Analyzed and interpreted the data; Contributed reagents, materials, analysis tools or data, Conceived and designed the experiments; Performed the experiments.

Keitaro Kondo: Analyzed and interpreted the data; Contributed reagents, materials, analysis tools or data; Conceived and designed the experiments.

Funding statement

The present work was performed in framework of the Broader Approach Agreement. The authors gratefully acknowledge the support of their home institutions and research funders in this work. Views and opinions expressed herein do not necessarily reflect those of QST, Fusion for Energy, or of the authors' home institutions or research funders.

Competing interest statement

The authors declare no conflict of interest.

Additional information

No additional information is available for this paper.

References

[1] M.R. Gilbert, et al., An integral model for materials in a fusion power plant: transmutation, gas production, and helium embrittlement under neutron irradiation, Nucl. Fusion 52 (2012) 083019.

[2] M.I. Norgett, et al., A proposed method of calculating displacement dose rates, Nucl. Eng. Des. 33 (1975) 50–54.

[3] M.R. Gilbert, et al., Neutron-induced dpa, transmutations, gas production, and helium embrittlement of fusion materials, J. Nucl. Mater. 442 (2013) S755–S760.

[4] P. Vladimirov, A. Moeslang, Comparison of material irradiation conditions for fusion, spallation, stripping, and fission neutron sources, J. Nucl. Mater. 329-333 (2004) 233–237.

http://dx.doi.org/10.1016/j.heliyon.2016.e00199

[5] S. Zinkle, A. Moeslang, Evaluation of irradiation facility options for fusion materials research and development, Fusion Eng. Des. 88 (6-8) (2013) 472–482.

[6] J. Knaster, et al., IFMIF, the European-Japanese efforts under the Broader Approach agreement towards a Li(d,xn) neutron Source: Current status and future options, Nucl. Mater. Energy (2016).

[7] J. Knaster, et al., The accomplishment of the Engineering Design Activities of IFMIF/EVEDA: The European-Japanese project towards a Li(d,xn) fusion relevant neutron source, Nucl. Fusion 55 (2015) 086003.

[8] J. Knaster, et al., IFMIF: overview of the validation activities, Nucl. Fusion 53 (2013) 116001.

[9] F. Arbeiter, et al., Design description and validation results for the IFMIF High Flux Test Module as outcome of the EVEDA phase, Nucl. Mater. Energy (2016).

[10] H. Kondo, et al., Validation of IFMIF liquid Li target for IFMIF/EVEDA project, Fusion Eng. Des. 96-97 (2015) 117–122.

[11] P. Cara, et al., The Linear IFMIF Prototype Accelerator (LIPAc) Design development under the European-Japanese collaboration, IPAC 16, Busan, Korea, 2016. www.jacow.org.

[12] R. Serber, The production of high energy neutrons by Stripping, Phys. Rev. 72 (1947).

[13] P. Grand, et al., An intense Li(d,n) neutron radiation test facility for controlled thermonuclear reactor materials testing, Nucl. Technol. 29 (1976) 327.

[14] A.L. Trego, et al., Fusion Materials Irradiation Test Facility - A facility for Fusion Materials Qualification, Nucl. Technol-Fusion 4 (2) (1983) 695.

[15] K. Noda, et al., Present status of ESNIT (energy selective neutron irradiation test facility) program, J. Nucl. Mater. 212-215 (1994) 1649–1654.

[16] P. Garin, Start of the engineering validation and design phase of IFMIF, J. Nucl. Mater. 386–388 (2009) 944.

[17] E.W. Pottmeyer Jr., The Fusion Material Irradiation Facility at Handford, J. Nucl. Mater. 85-86 (1979) 463–465.

[18] J. Knaster, et al., Assessment of the beam–target interaction of IFMIF: A state of the art, Fusion Eng. Des. 89 (2014) 1709–1716.

[19] F. Mota, et al., Sensitivity of IFMIF-DONES irradiation characteristics to different design parameters, Nucl. Fusion 55 (12) (2015) 123024.

 http://dx.doi.org/10.1016/j.heliyon.2016.e00199

[20] G. Micciche, et al., Analysis of the thermomechanical behavior of the IFMIF bayonet target assembly under design loading scenarios, Fusion Eng. Des. 96-97 (2015) 217–221.

[21] F. Nitti, et al., The design status of the liquid lithium target facility of IFMIF at the end of the engineering design activities, Fusion Eng. Des. 100 (November 2015) 425–430.

[22] H. Kondo, et al., Completion of IFMIF/EVEDA Lithium Test Loop Construction, Fusion Eng. Des. 87 (2012) 418–422.

[23] H. Kondo, et al., Measurement of cavitation in a downstream conduit of the liquid lithium target for IFMIF, Proceedings of ICONE 23, May 2015 Chiba, Japan (2016).

[24] T. Kanemura, et al., Measurement of Li target thickness in the EVEDA Li Test Loop, Fusion Eng. Des. 98-99 (2015) 1991–1997.

[25] J.A. Hassberger, Preliminary Assessment of Interactions Between the FMIT Deuteron Beam and Liquid Lithium Target, HEDL-TME 82-28, Hanford Engineering Development Laboratory, Richland WA (March 1983).

[26] A. Hassanein, Deuteron beam interaction with lithium jet in a neutron source test facility, J. Nucl. Mater. 233–237 (1996) 1547–1551.

[27] Y. Momozaki, et al., Proton beam-on-liquid lithium stripper film experiment, J. Radioanal. Nucl. Chem. (April 2015).

[28] P.J. Brackenbury, et al., The Fusion Materials Irradiation Test (FMIT) Facility Lithium System - A Design and Development Status, Fusion Sci. Technol. 4 (2P2) (September 1983) 724–729.

[29] H. Kondo, et al., IFMIF/EVEDA Lithium Test Loop: Design and Fabrication Technology of Target Assembly as a Key Component, Nucl. Fusion 51 (2011) 123008.

[30] N. Loginov, The thermal-hydraulic and technological investigations for validation of the project of lithium circulation loop and neutron lithium target for IFMIF, Final Report on Research and Development Activities on #2036 ISTC Project, IPPE, Obninsk, 2006.

[31] T. Kanemura, et al., Analytical and experimental study of rate of evaporation from high-speed liquid lithium jet, J. Nucl. Mater. (2017).

[32] I. Langmuir, Vapour pressures, evaporation, condensation and adsorption, J. Am. Chem. Soc. 54 (7) (1932) 2798–2832.

 http://dx.doi.org/10.1016/j.heliyon.2016.e00199

[33] H. Hertz, Üer die Verdunstung der Flussigkeiten inbesondere des Quecksilbers, im lufteeren Raume, Ann. Phys. Chem. 17 (1882) 177–200.

[34] M. Knudsen, Die Maximale Verdampfungs geschwindigkeit des Quecksilbers, Ann. Phys. Chem. 47 (1915) 697–708.

[35] I. Langmuir, The Condensation and Evaporation of Gas Molecules, Proc. Natl. Acad. Sci. USA 3 (3) (March 15, 1917) 141–147.

[36] I.W. Eames, et al., The evaporation coefficient of water: a review, Int. J. Heat Mass Transfer 40 (12) (1997) 2963–2973.

[37] J. Stefan, Versuche uber die Verdampfung Sitzungsber, Kais, Akad. Wiss. Wien. Math. Naturwiss. Kl., Abt. IIa68 (1873) 385–423.

[38] J. Safaranian, T.A. Engh, Vacuum Evaporation of Pure Metals, Metall. and Mat. Trans. A 44A (2013) 747.

[39] J.P. Hirth, G.M. Pond, Condensation and Evaporation, Prog. Mater. Sci. (1963) Vol. XI, Pergamon, Oxford.

[40] S.H. Algie, Vacuum evaporation from finite surfaces, Vacuum 26 (12) (1976).

[41] Z.J. Wang, et al., A non-equilibrium molecular dynamics simulation of evaporation, International Conference Passive and Low Energy Cooling for the Built Environment 2005, Santorini, Greece (2016).

[42] R.W. Schrage, A Theoretical Study of Interphase Mass Transfer, Columbia University Press, New York, 1953.

[43] G. Standart, Z. Cihla, Interphase transport processes I, Schrage's theories, Collect. Czech. Chem. Commun. 23 (1958) 1608–1618.

[44] P. Rahimi, C.A. Ward, Kinetics of evaporation: Statistical rate theory approach, Int. J. Thermo. 8 (1) (March 2005) 1–14.

[45] V.V. Semak, Atomistic misconception of current model for condensed matter evaporation and new formulation, Cornell University Library, 2016 arXiv:1406.2261v1.

[46] D.A. Labuntsov, A.P. Kryukov, Processes of intense evaporation, Int. J. Heat Mass Transfer. 22 (1979) 989–1002.

[47] L.D. Koffman, M.S. Plesset, L. Lees, Theory of evaporation and condensation, Phys. Fluids 27 (1984) 876–880.

[48] T. Ytrehus, S. Østmo, Qualitative analysis of the Navier-Stokes equations for evaporation-condensation problems, Int. J. Multiph. Flow 22 (1996) 133–155.

 http://dx.doi.org/10.1016/j.heliyon.2016.e00199

[49] S. Brunauer, et al., On a Theory of the van der Waals Adsorption of Gases, J. Am. Chem. Soc. 62 (7) (1940) 1723–1732.

[50] S. Brunauer, P.H. Emmett, E. Teller, Adsorption of Gases in Multimolecular Layers, J. Am. Chem. Soc. 60 (2) (1938) 309–319.

[51] A. Ibarra, et al., A stepped Approach from IFMIF/EVEDA toward IFMIF, Fusion Sci. Technol. 66 (2014) 252–259.

[52] T. Nishitani, et al., DEMO activities in the Broader Approach and beyond, Fusion Sci. Technol. 66 (2014) 1–8.

[53] J.A. Nolen, et al., Behaviour of liquid lithium jet irradiated by 1 MeV electron beam up to 20 kW, Rev. Sci. Instrum. 76 (2005) 073501.

[54] J. Knaster, et al., IFMIF, a fusion relevant neutron source for material irradiation current status, J. Nucl. Mater. 453 (1-3) (2014) 115–119.

[55] J. Knaster, Y. Okumura, Accelerators for fusion materials testing, Rev. Accel. Sci. Technol. 8 (2015) 115–142.

[56] J. Knaster, et al., Materials research for fusion, Nature Phys. 12 (2016) 424.

 http://dx.doi.org/10.1016/j.heliyon.2016.e00199